From longitudinal slab curvature to slab rheology

Christelle Loiselet*, Laurent Husson, and Jean Braun
Geosciences Rennes, UMR 6118 CNRS, Université de Rennes 1, Rennes Cedex CS 35042, France

ABSTRACT

The curvature of a subducting lithosphere is chiefly controlled by the viscosity ratio between the slab and the surrounding mantle. On the basis of a semi-analytical flow model, we explore the rheological dependence of the geometrical response of a viscous slab subjected to toroidal mantle flow. Mantle flow is excited by slab retreat at a prescribed mean velocity and is iteratively solved for by using a stream function approach, in turn providing the stresses that bend the slab. Comparison between model predictions and geophysical observations of slab curvature gives an average slab-to-mantle viscosity ratio of 45.

INTRODUCTION

Much effort has been recently devoted to improve our understanding of the dynamics of subduction zones; surprisingly, the viscosity of the subducting lithosphere remains a poorly known yet fundamental parameter. Modeling subduction dynamics (e.g., Billen and Hirth, 2007; Capitanio et al., 2007; Wu et al., 2008) or the geoid (e.g., Zhong and Davies, 1999) has led to a wide range of values. We take advantage of the dependence of slab curvature on the viscosity ratio between the slab and the mantle to determine this ratio by studying the response of a retreating slab in a longitudinal plane (i.e., perpendicular to the slab plane at a given depth) exciting a toroidal mantle flow. By means of a semi-analytical method, we quantify the mechanical behavior of the slab and compare our model results with observations from geophysical data on a selection of subduction zones.

GEOMETRY AND RHEOLOGY OF SLABS

The interaction between a subducting lithosphere and the surrounding mantle is strongly affected by their relative strengths. For example, whether slabs penetrate the lower mantle is controlled by the strength of the lithosphere in comparison with the viscosity structure of the mantle at the 660 km discontinuity (Goes et al., 2008). Commonly used values for the viscosity ratio between a slab and the surrounding mantle range between 10^2 and 10^5 (Christensen and Yuen, 1984; Zhong and Gurnis, 1994; Conrad and Hager, 1999; Funiciello et al., 2003; Schellart, 2004; Morra et al., 2006; Royden and Husson, 2006; Stegman et al., 2006; Billen and Hirth, 2007; Capitanio et al., 2007; Clark et al., 2008), but Kincaid and Griffiths (2004) modeled the flow around a rigid slab, while Husson (2006) reproduced observations of dynamic topography with an isoviscous rheology.

Most oceanic trenches have a convex arc shape, a feature that is not limited to surface level. Seismic tomography studies as well as earthquake occurrences provide information on the geometry of subducted slabs (Isacks and Molnar, 1971; Van der Hilst and Karason, 1999; Wortel and Spakman, 2000; Fukao et al., 2001). The shape of ocean trenches was first explained by the ping-pong ball analogy (Frank, 1968; Tovish and Schubert, 1978), which suggested that the curvature of the trenches is naturally imposed by the intersection of a slab and a spherical Earth. Alternatively, numerical and analogue simulations have shown that this curvature is more likely the response of the slab in a toroidal flow. This curvature seems to decrease when slab width increases (Dvorkin et al., 1993; Morra et al., 2006, 2009; Stegman et al., 2006; Schellart et al., 2007), as a response to the balance between the forces driving slab motion and the viscous resistance of the mantle (Schellart, 2004; Funiciello et al., 2006), although internal heterogeneities may have a strong impact (Morra et al., 2006).

Because the flow associated with a migrating slab is predominantly toroidal (e.g., Schellart, 2004; Funiciello et al., 2006; Piromallo et al., 2006), we assume that the time evolution of the shape of a vertical slab that retreats at a given rate can be directly compared to the depth evolution of the longitudinal shape of a slab; this operation can be performed via the conversion of depth along slab into a residence time into the mantle, calculated as the depth divided by the sinking velocity (assuming that retreat velocity, and therefore slab dip, is constant with depth).

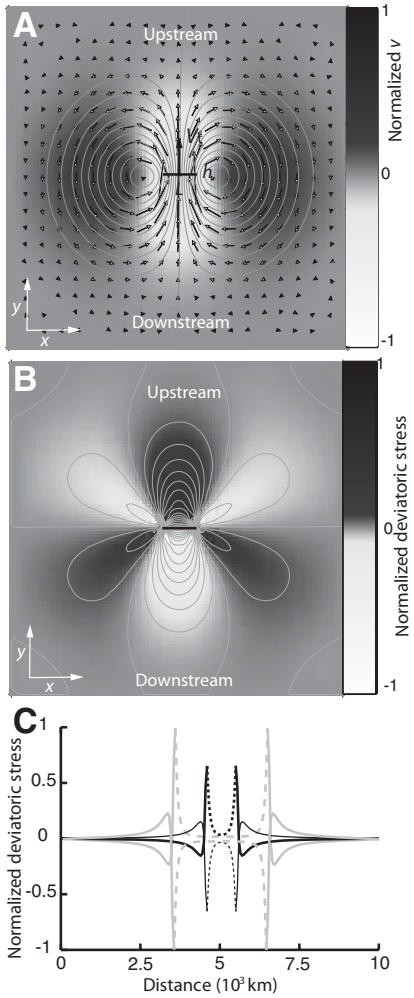

Figure 1. Map view of model. A: Normalized streamlines (gray curves), velocity field (arrows), and *v*, velocity field, parallel to *y* axis (background). V_t is translation velocity of slab. *L* and *h* are slab width and thickness. B: Normalized deviatoric stress, isocurves every 0.05. C: Deviatoric stress profile along line parallel to *x* axis and running on upstream (bold) and downstream (thin) side of 1000 km (black) and 3000 km (gray) plate across model. Dashed sections denote stresses along slab.

MODELING APPROACH

The retreating slab is approximated by a uniform infinite vertical viscous layer of variable width L and thickness h moving in a square domain of constant dimensions throughout (Fig. 1A). Our approach is based on a two-dimensional (2-D) numerical solution of the Stokes equation that requires the computation of (1) a stream function to describe the toroidal flow of a Newtonian, isoviscous, and incompressible mantle around a rigid retreating plate, infinite in the direction perpendicular to the model (2-D), and (2) from the resulting stress field, the deflection of a viscous slab of uniform yet different viscosity. The velocity of the fluid is obtained by solving the biharmonic equation for the stream function Ψ, $\nabla^4\Psi = 0$, with $u = -\frac{\partial\Psi}{\partial y}$ and $v = \frac{\partial\Psi}{\partial x}$, u and v being the x and y velocities, respectively. To simulate the presence of the retreating slab, we prescribe a velocity V_t (slab retreat rate) in

*E-mail: christelle.loiselet@univ-rennes1.fr.

a rectangular region of width L and thickness h in the center of the model (Fig. 1A), while the velocities at the boundaries of the domain are set to zero. We then calculate Ψ at the nodes of a regular grid using a centered finite difference operator to approximate the spatial derivatives. In the first step of the model, we assume that the slab is rigid, and iteratively solve for the velocity field that minimizes work while satisfying the incompressibility condition.

The deflection of the slab is obtained in a second step by solving for the viscous bending of a half-plate embedded at its origin (and by symmetry, for the entire plate), of thickness h and length $L/2$, and subjected to a nonuniform load $q(x)$ (or spatially integrated deviatoric stress):

$$D\frac{\partial^5 w}{\partial x^4 \partial t} = q(x), \qquad (1)$$

where $D = \frac{\mu_s h^3}{3}$ is the viscous rigidity of the slab, μ_s the slab viscosity, and $q(x) = \mu_m \frac{\partial u}{\partial x}$ is the deviatoric stress induced by the mantle flow. The approximation is made that $\sigma_{yy} = 0$, which only holds when the slab viscosity is larger than the mantle viscosity μ_m. The deflection w of the half-plate as a function of time t and x is given by the integration of Equation 1. Standard boundary conditions are $w = 0$ and $\frac{dw}{dx} = 0$ at $x = 0$; $\frac{d^2w}{dx^2} = 0$ and $\frac{d^3w}{dx^3} = 0$ at $x = L/2$ (Turcotte and Schubert, 1982). The slab geometry is modified according to the computed final displacement after each time increment (small enough for the solution to become independent of its value). The coupled equations are iteratively solved through time in order to predict the evolving plate curvature.

We dimensionalized the model by assigning a mean slab retreat rate V_t = 50 mm/a in a 10,000-km-wide square box filled with a linear viscous fluid of viscosity 10^{20} Pa s. Note that in a Newtonian viscous fluid, the flow pattern does not depend on the absolute value of the viscosity, but rather on the viscosity ratios. Thus, if the imposed velocity is twice as large, we obtain the same velocity field but at twice the amplitude. Equation 1 breaks down when the viscosity ratio is too low; we must ensure that the slab rigidity is sufficiently large for the deflection to be inferior or equal to the slab displacement, which puts a minimum bound on the allowable viscosity ratio.

RESULTS

The resulting flow pattern (Fig. 1A) shows a pair of symmetrical toroidal cells, one on each side of the slab, focused close to the plate edges. Velocities are maximum just upstream and downstream of the plate (most positive values) and close to the slab edges (most negative values). On the sides of the slab, the negative y velocity is the return flow. Slab retreat results in compression along the upstream side of the slab and extension along the downstream side of the slab (Fig. 1B). The stress pattern also shows two opposite-sign ear-shape anomalies, on either side of the slab, of amplitudes proportional to the slab width. It is interesting that maximum stresses are found close to the slab edges (Fig. 1C); away from the slab edges, the stress field abruptly reverts and becomes extensional (negative) on the upstream side and compressive (positive) on the downstream side. Near the center of the slab, the deviatoric stresses diminish and tend toward zero (Fig. 1C). In all experiments, slab deformation is concentrated along its edges, where stresses are maximum. This surprising stress distribution (see also Morra et al., 2006) is responsible for slab curvature along their edges. As time progresses, the slab geometry evolves at a rate that is dictated by the slab to mantle viscosity ratio.

We performed a series of experiments in which the slab was alternatively 500, 1000, and 2000 km wide and 50, 100, and 200 km thick. For each experiment, the viscosity ratio between the slab and surrounding mantle was systematically changed to encompass the desired range. The system is bounded by the no-velocity conditions along the edges of the box, and the behavior of the slab depends on the box width to slab dimension ratio. This condition mimics real Earth conditions, where subduction zones are embedded in the finite terrestrial system.

We characterize slab curvature from a quadratic regression on the slab shape. After a mean retreat of 1000 km, the coefficient of curvature C of the slab (defined as the quadratic coefficient of a quadratic polynomial function fit) varies between 10^{-4} and 6 10^{-3} km^{-1} (Fig. 2). In all cases, curvature is inversely proportional to the viscosity ratio [$C \sim 1/(\mu_s/\mu_m)$], with the lowest ratio leading to the highest curvature, as imposed by the above equation for flexure. As slabs widen, the stresses in the fluid during slab retreat become high because free space around the slab decreases. Consequently, wide slabs get highly loaded and slab curvature increases accordingly. Slab rigidity varies as the cube of slab thickness, the thicker the slab the smaller the curvature, and our models accordingly yield $C \sim h^{-3}$.

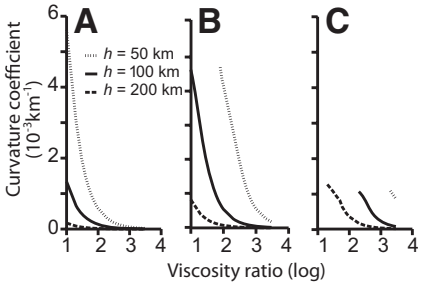

Figure 2. Slab coefficient of curvature (see text) as function of lithosphere to surrounding mantle viscosity ratio. Slab is alternatively 50 (dotted), 100 (solid), and 200 km (dashed) thick (*h*) and 500 (A), 1000 (B), and 2000 (C) km wide, respectively. Some curves are truncated when initial model assumptions no longer hold (see text).

COMPARISON TO REAL EARTH

The curvature of narrow slabs (e.g., Scotia, Calabria, Hellenic) is larger than that of wider slabs (e.g., Aleutian, South America, Java, Tonga). In order to determine the shape of slabs at depth, we use the results of P-wave seismic tomography (Li et al., 2008) and catalogues of earthquake locations (International Seismological Centre, 2008; Engdahl et al., 1998) for four subduction systems (Aleutians, Scotia, Hellenic, and Calabria) selected for the variety of width, thickness, and retreat velocity they present. We also compare our interpretation to the slab geometries derived from the RUM (regionalized upper mantle) model (Gudmundsson and Sambridge, 1998). In practice we mapped the tomographic model on a Cartesian grid, together with seismicity and the RUM slab geometry. We estimated slab curvature by contouring the fast seismic velocity anomalies. We measured the curvature between 50 and 700 km in the upper mantle, every 50 km. Because the depth along the subducted lithosphere correlates with a residence time in the mantle, i.e., the time during which the section of the slab entered the subduction zone and experienced the pressure field from the surrounding mantle, we expect the curvature of a viscous slab to increase with depth. One should, however, be careful in estimating slab curvature for very wide slabs, because other factors, such as the age of the lithosphere, the nature of the overriding plate, the presence of seamounts or oceanic plateaus in the subduction zone (Nur and Ben-Avraham, 1982), and possibly more important, the aspect ratio between upper mantle thickness and slab width, could affect the curvature of the slab near the surface.

We match observations to model results by computing the flow around the slab using kinematic and geometric characteristics of each natural system. Because trench velocity depends on the reference frame, we consider the Indo-Atlantic (O'Neill et al., 2005) and Pacific (Gripp and Gordon, 2002) hotspot reference frames, as well as the no-net-rotation frame (Kreemer et al., 2003). Trench migration rates are from Schellart et al. (2008) (Table 1). The slab-to-mantle viscosity ratio is therefore the remaining free parameter that we vary until

TABLE 1. KINEMATIC AND GEOMETRICAL CHARACTERISTICS OF THE SUBDUCTION SYSTEMS AND BEST-FIT SLAB-TO-MANTLE VISCOSITY RATIOS

	Velocity (mm a–1) Vs	Velocity (mm a–1) IA Vt	Velocity (mm a–1) HS3 Vt	Velocity (mm a–1) NNR Vt	Slab thickness (km)	Slab width (km)	μs/μm IA	μs/μm HS3	μs/μm NNR
Aleutian	71	12	–5	21	100	3000	40	*	80
Scotia	74	57	40	94	70	1000	60	50	100
Hellenic	44	23	51	10	100	1100	40	60	30
Calabria	68	68	52	10	100	600	10	5	1

Note:The trench–perpendicular trench migration rate (i.e., *Vt*, slab retreat rate) (trench retreat is taken as positive) and Vs, the velocity of the subducting plate in three global reference frames. IA—Indo-Atlantic hotspot reference frame (O'Neill et al., 2005); HS3—Pacific hotspot reference frame (Gripp and Gordon, 2002); NNR—no-net-rotation reference frame of Kreemer et al. (2003). μs/μm is the viscosity ratio between slab and surrounding mantle obtained by the best fit between model and natural data for each global reference frame. Kinematic values are from Schellart et al. (2007). Trench length is measured after Gudmundsson and Sambridge (1998).

*Observed slab curvature is incompatible with Aleutian trench advance in this reference frame.

the modeled and observed curvatures match (Fig. 3). In all cases the domain is 10,000 km wide, which may induce a systematic bias, because we do not know what the most appropriate dimension would be for Earth. This recurrent issue relates to the Stokes paradox (Lamb, 1932). Nonetheless, the slab to box edge distance (5000 km) is comparable to the characteristic distance that separates slabs from each other on Earth.

The estimated viscosity ratio varies between 1 and 100 (Table 1). We note that for narrow slabs (Scotia and Calabria slabs; Figs. 3B and 3D), slab curvature strongly increases with depth. For Calabria, the strong curvature is best fitted by using a slightly lower viscosity ratio, which may be consistent with local geodynamics (Faccenna et al., 2007). Wider slabs are characterized by a lower curvature (Figs. 3A and 3C) but the best-fit viscosity ratio is in the same range (40–80) as the narrower Scotia slab, also suggesting that the slab width-to-length ratio primarily controls slab curvature. In all cases, the RUM model leads to grossly overestimated slab curvature except for the wide Aleutian slab.

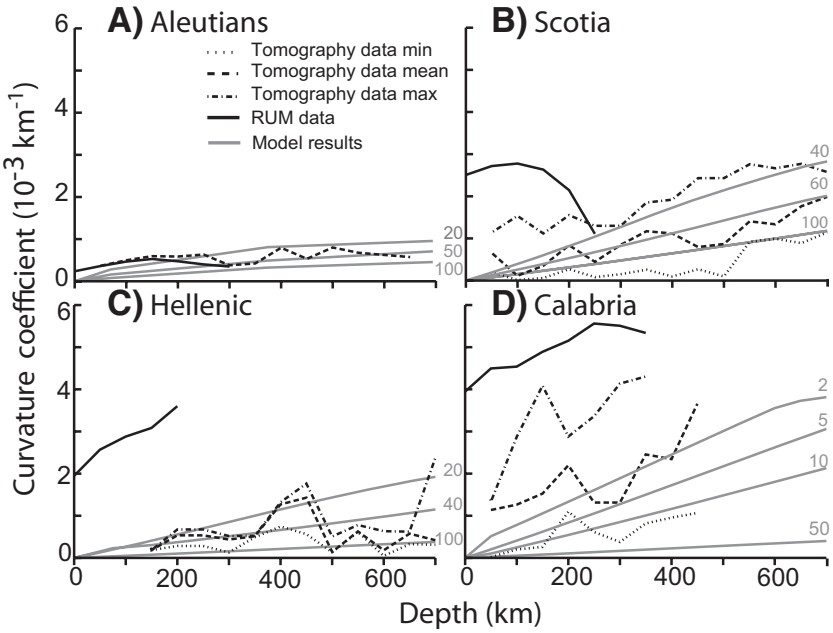

Figure 3. Evolution of predicted (gray curves) and observed (from geophysical data, black curves: minimum—dotted; mean—dashed; and maximum—dotted-dashed) coefficient of curvature of slab (see text) as function of depth for several viscosity ratios between slab and upper mantle, for Aleutian (A), Scotia (B), Hellenic (C), and Calabria (D) subduction zones (for Indo-Atlantic reference frame). Geophysical data used include global P-wave seismic tomography model (Li et al., 2008), location of seismic events from International Seismological Centre (2008) catalog, database published by Engdahl et al. (1998), and RUM (regionalized upper mantle) model for global slab geometry (Gudmundsson and Sambridge, 1998).

DISCUSSION AND CONCLUSION

Slab motion is primarily driven by the negative buoyancy of the slab with respect to the ambient mantle and is controlled to a large extent by slab width. The toroidal component of mantle circulation, unaccounted for in 2-D models, plays a key role in shaping the slab. Increasing slab width confines the toroidal flow into a constant size domain. It decreases trench velocity and the vigor of the mantle flow, and generates a higher stress field in the fluid, and ultimately a higher rate of viscous energy dissipation (Fig. 4B). Consequently, slab width also tends to inhibit trench retreat (Schellart, 2004; Stegman et al., 2006) (Fig. 4A), and, at a given stage in the temporal evolution of the slab, slab curvature will be lower for a wide slab than for a narrow one. Although the buoyancy of a slab is linearly proportional to its width, because the viscous dissipation increases as a power law of slab width in a mantle of finite dimension (Fig. 4B), the resisting force will ultimately dominate and large slabs will retreat at slower rates than small ones as an indirect consequence of the Stokes paradox (Lamb, 1932). Thus, these results in turn explain why narrow slabs (e.g., Calabria or Scotia) retreat faster (Fig. 4A) than wider ones. Our assumption that the surface is implicitly stress free (2-D approximation) affects our results (e.g., Jarvis and Lowman, 2005), as does the no-slip lateral boundary condition that will influence the flow pattern (e.g., Piromallo et al., 2006) and accentuate the Stokes paradox effect.

The comparison of theoretical computations with natural slab curvature independently delimits the viscosity ratio between the subducted lithosphere and the surrounding mantle to range from 1 to 100, with an average of ~45,

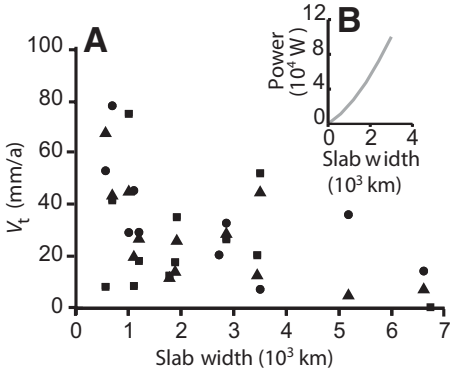

Figure 4. A: Average trench-perpendicular migration rate (V_t is slab retreat rate) as function of slab width in Pacific (circles, Gripp and Gordon, 2002) and Indo-Atlantic (triangles, O'Neill et al., 2005) hotspot reference frames, as well as in no-net-rotation model of Kreemer et al. (2003) (squares). Data are from Schellart et al. (2008). B: Predicted energy dissipation rate (power) as function of slab width.

smaller by a factor of 2 (Capitanio et al., 2007) to more than 10^4 (Billen and Hirth, 2007) compared to previous estimates. In other words, if the upper mantle viscosity is assumed to be 10^{20} Pa s, slab viscosity is in the range 10^{20}–10^{22} Pa s, with a mean value of 4.5×10^{21} Pa s. The choice of the reference frame may change the values of the viscosity ratio by a factor of 2 (Table 1; comparable to Funiciello et al., 2008). However, because the azimuthal distribution of trenches on Earth is approximately even, mean retreat rates, and therefore the mean viscosity ratios, should be independent of the reference frame.

ACKNOWLEDGMENTS

We thank W. Royden, F. Chambat, P. Yamato, and B. Huet for stimulating discussions. Loiselet and Braun acknowledge funding from the Agence National de la Recherche (ANR), and Husson from the Institut National des Sciences de l'Univers–Centre National de la Recherche Scientifique (INSU/CNRS) program "SEDIT." We thank editor S. Wyld, and F. Funiciello, W. Schellart, and an anonymous reviewer for constructive reviews.

REFERENCES CITED

Billen, M.I., and Hirth, G., 2007, Rheologic controls on slab dynamics: Geochemistry Geophysics Geosystems, v. 8, Q08012, doi: 10.1029/2007GC001597.

Capitanio, F.A., Morra, G., and Goes, S., 2007, Dynamic models of downgoing plate-buoyancy driven subduction: Subduction motions and energy dissipation: Earth and Planetary Science Letters, v. 262, p. 284–297, doi: 10.1016/j.epsl.2007.07.039.

Christensen, U., and Yuen, D., 1984, The interaction of a subducted lithosphere slab with a chemical or phase boundary: Journal of Geophysical Research, v. 89, p. 4389–4402, doi: 10.1029/JB089iB06p04389.

Clark, S.R., Stegman, D., and Muller, R.D., 2008, Episodicity in back-arc tectonic regimes: Physics of the Earth and Planetary Interiors, v. 171, p. 265–279, doi: 10.1016/j.pepi.2008.04.012.

Conrad, C.P., and Hager, B.H., 1999, Effect of plate bending and fault strength at subduction zones on plate dynamics: Journal of Geophysical Research, v. 104, p. 17,551–17,571, doi: 10.1029/1999JB900149.

Dvorkin, J., Nur, A., Mavko, G., and Ben-Avraham, Z., 1993, Narrow subducted slabs and the origin of backarc basins: Tectonophysics, v. 227, p. 63–79, doi: 10.1016/0040-1951(93)90087-Z.

Engdahl, E.R., van der Hilst, R., and Buland, R., 1998, Global teleseismic earthquake relocation with improved travel times and procedures for depth determination: Seismological Society of America Bulletin, v. 88, p. 722–743.

Faccenna, C., Civetta, L., Massimo, D.A., Moroni, M., and Piromallo, C., 2007, Slab disruption, mantle circulation, and the opening of the Tyrrhenian basins, *in* Beccaluva, L., et al., eds., Cenozoic volcanism in the Mediterranean area: Geological Society of America Special Paper 418, p. 153–169, doi: 10.1130/2007.2418(08).

Frank, F.C., 1968, Curvature of island arcs: Nature, v. 220, p. 363, doi: 10.1038/220363a0.

Fukao, Y., Widiyantoro, S., and Obayashi, M., 2001, Stagnant slabs in the upper and lower mantle transition region: Reviews of Geophysics, v. 39, p. 291–323, doi: 10.1029/1999RG000068.

Funiciello, F., Faccenna, C., Giardini, D., and Regenauer-Lieb, K., 2003, Dynamics of retreating slab: 2. Insights from three-dimensional laboratory experiments: Journal of Geophysical Research, v. 108, 2207, doi: 10.1029/2001JB000896.

Funiciello, F., Moroni, M., Piromallo, C., Faccenna, C., Cenedese, A., and Bui, H.A., 2006, Mapping mantle flow during retreating subduction: Laboratory models analyzed by feature tracking: Journal of Geophysical Research, v. 111, B03402, doi: 10.1029/2005JB003792.

Funiciello, F., Faccenna, C., Heuret, A., Lallemand, S., Di Giuseppe, E., and Becker, T.W., 2008, Trench migration, net rotation and slab-mantle coupling: Earth and Planetary Science Letters, v. 271, p. 233–240, doi: 10.1016/j.epsl.2008.04.006.

Goes, S., Capitanio, F., and Morra, G., 2008, Evidence of lower-mantle slab penetration phasesin plate motions: Nature, v. 451, p. 981–984, doi: 10.1038/nature06691.

Gripp, A.E., and Gordon, R.G., 2002, Young tracks of hotspots and current plate velocities: Geophysical Journal International, v. 150, p. 321–361, doi: 10.1046/j.1365-246X.2002.01627.x.

Gudmundsson, O., and Sambridge, M., 1998, A regionalized upper mantle (RUM) seismic model: Journal of Geophysical Research, v. 103, p. 7121–7136, doi: 10.1029/97JB02488.

Husson, L., 2006, Dynamic topography above retreating subduction zones: Geology, v. 34, p. 741–744, doi: 10.1130/G22436.1.

International Seismological Centre, 2008, Regional catalog of earthquakes: International Seismological Centre, http://www.isc.ac.uk/doc/products/catalogue.html.

Isacks, B., and Molnar, P., 1971, Distribution of stresses in the descending lithosphere from a global survey of focal mechanism solutions of mantle earthquakes: Reviews of Geophysics, v. 9, p. 103–174, doi: 10.1029/RG009i001p00103.

Jarvis, G.T., and Lowman, J.P., 2005, Sinking slabs below fossil subduction zones: Physics of the Earth and Planetary Interiors, v. 152, p. 103–115, doi: 10.1016/j.pepi.2005.05.002.

Kincaid, C., and Griffiths, R.W., 2004, Variability in flow and temperatures within mantle subduction zones: Geochemistry Geophysics Geosystems, v. 5, p. Q06002, doi: 10.1029/2003GC000666.

Kreemer, C., Holt, W.E., and Haines, A.J., 2003, An integrated global model of present-day plate motions and plate boundary deformation: Geophysical Journal International, v. 154, p. 8–34, doi: 10.1046/j.1365-246X.2003.01917.x.

Lamb, H., 1932, Hydrodynamics (sixth edition): Cambridge, Cambridge University Press, 768 p.

Li, C., van der Hilst, R.D., Engdahl, E.R., and Burdick, S., 2008, A new global model for P wave speed variations in Earth's mantle: Geochemistry Geophysics Geosystems, v. 9, p. 157–168, doi: 10.1016/j.epsl.2008.07.016.

Morra, G., Regenauer-Lieb, K., and Giardini, D., 2006, Curvature of oceanic arcs: Geology, v. 34, p. 877–880, doi: 10.1130/G22462.1.

Morra, G., Chatelain, P., Tackley, P., and Koumoutzakos, P., 2009, Earth curvature effects on subduction morphology: Modeling subduction in a spherical setting: Acta Geotechnica, doi: 10.1007/s11440-008-0060-5.

Nur, A., and Ben-Avraham, Z., 1982, Oceanic plateaus, the fragmentation of continents, and mountain building: Journal of Geophysical Research, v. 87, p. 3644–3661, doi: 10.1029/JB087iB05p03644.

O'Neill, C., Muller, D., and Steinberger, B., 2005, On the uncertainties in hot spot reconstructions and the significance of moving hot spot reference frames: Geochemistry Geophysics Geosystems, v. 6, Q04003, doi: 10.1029/2004GC000784.

Piromallo, C., Becker, T.W., Funiciello, F., and Faccenna, C., 2006, Three-dimensional instantaneous mantle flow induced by subduction: Geophysical Research Letters, v. 33, doi: 10.1029/2005GL025390.

Royden, L.H., and Husson, L., 2006, Trench motion, slab geometry and viscous stresses in subduction systems: Geophysical Journal International, v. 167, p. 881–905, doi: 10.1111/j.1365-246X.2006.03079.x.

Schellart, W.P., 2004, Kinematics of subduction and subduction-induced flow in the upper mantle: Journal of Geophysical Research, v. 109, B07401, doi: 10.1029/2004JB002970.

Schellart, W.P., Freeman, J., Stegman, D.R., Moresi, L., and May, D., 2007, Evolution and diversity of subduction zones controlled by slab width: Nature, v. 446, p. 308–311, doi: 10.1038/nature05615.

Schellart, W.P., Stegman, D.R., and Freeman, J., 2008, Global trench migration velocities and slab migration induced upper mantle volume fluxes: Constraints to find an Earth reference frame based on minimizing viscous dissipation: Earth-Science Reviews, v. 88, p. 118–144, doi: 10.1016/j.earscirev.2008.01.005.

Stegman, D.R., Freeman, J., Schellart, W.P., Moresi, L., and May, D., 2006, Influence of trench width on subduction hinge retreat rates in 3-D models of slab rollback: Geochemistry Geophysics Geosystems, v. 7, Q03012, doi: 10.1029/2005GC001056.

Tovish, A., and Schubert, G., 1978, Island arc curvature, velocity of convergence and angle of subduction: Geophysical Research Letters, v. 5, p. 329–332, doi: 10.1029/GL005i005p00329.

Turcotte, D.L., and Schubert, G., 1982, Geodynamics: Application of continuum physics to geological problem: New York, John Wiley and Sons, 450 p.

Van der Hilst, R., and Karason, H., 1999, Compositional heterogeneity in the bottom 1000 kilometers of Earths mantle: Toward a hybrid convection model: Science, v. 283, p. 1885–1888, doi: 10.1126/science.283.5409.1885.

Wortel, M.J.R., and Spakman, W., 2000, Subduction and slab detachment in the Mediterranean-Carpathian region: Science, v. 290, p. 1910–1917, doi: 10.1126/science.290.5498.1910.

Wu, B., Conrad, C.P., Heuret, A., Lithgow-Bertelloni, C., and Lallemand, S., 2008, Reconciling strong slab pull and weak plate bending: The plate motion constraint on the strength of mantle slabs: Earth and Planetary Science Letters, v. 272, p. 412–421, doi: 10.1016/j.epsl.2008.05.009.

Zhong, S., and Davies, G.F., 1999, Effects of plate and slab viscosities on the geoid: Earth and Planetary Science Letters, v. 170, p. 487–496, doi: 10.1016/S0012-821X(99)00124-7.

Zhong, S., and Gurnis, M., 1994, Controls on trench topography from dynamic models of subducted slabs: Journal of Geophysical Research, v. 99, p. 15,683–15,695, doi: 10.1029/94JB00809.

Manuscript received 21 January 2009
Revised manuscript received 24 March 2009
Manuscript accepted 1 April 2009

Printed in USA